

Quasi 3D model for numerical computations of screening currents in REBCO coils

Philippe Fazilleau and Guillaume Dilasser CEA, Université Paris-Saclay, 91191 Gif-sur-Yvette, France.

Abstract—Screening currents are a major drawback in the context of REBCO magnets due to their parasitic effects on the generated field being exacerbated by the particular shape of the conductors. Previously, we have developed numerical tools for the computation of screening currents and their effects in the cases of systems featuring 2D symmetries, axial or longitudinal. Nevertheless, 2D models are not always adequate for every 3D shapes or alternative winding configurations, like layer-wound ones.

Therefore, a quasi three-dimensional model has been implemented in the in-house CAST3M finite element code, using the current function \mathbf{T} formulation. We developed CAST3M operators to take into account the superconducting behavior of the material and the anisotropic dependence of the current density on the magnetic induction.

Simple scenarios, especially one solved with analytical formulations, have been defined to benchmark codes; CASTEM was successfully benchmarked against them.

Finally, we compared the generation of screening currents within a small solenoid depending on the type of winding, made either of layers or pancakes. We also compared these results with a simple 2D model made of nested turns.

Index Terms—HTS coil, layer winding, pancake winding, screening currents.

I. INTRODUCTION

THE development of HTS magnets has been growing during the last few years, especially using the new HTS coated conductors. HTS magnets or magnet prototypes are available in several fields of application such as accelerators magnets [1], high-field magnets [2] and medical applications, NMR or MRI magnets [3].

Several issues have come to light with these new conductors, especially regarding quench protection and magnetic field homogeneity. Our article focuses on this latter subject as their particular tape shape makes them very sensitive to orthogonal magnetic field variations resulting in large screening currents.

The screening currents have three main unwanted effects on the total magnetic field: they lower its amplitude at the center of the magnet that is often the most important parameter for practical applications, they degrade its homogeneity and induce a temporal drift.

Therefore, it is important to estimate the impact of these unwanted effects on the magnetic field and homogeneity by calculating the Screening Current Induced Field (SCIF).

In order to calculate the SCIF, we need to solve the problem with one or two state variables. Several methods are used with different state variables, such as the current density \mathbf{J} , the

magnetic field \mathbf{H} [4], the (\mathbf{T}, Φ) formulation [5], with the current vector potential \mathbf{T} and the magnetic scalar potential Φ or the (\mathbf{A}, V) formulation [6] with the vector potential \mathbf{A} and the electrical scalar potential V .

In previous articles, we developed and benchmarked numerical tools for the computation of screening currents and their effects in the cases of systems featuring 2D symmetries, axial or longitudinal using (\mathbf{A}, V) formulation [7] or \mathbf{H} formulation [8][9]. Nevertheless, 2D models are not always adequate for all 3D shapes or alternative winding configurations, such as layers.

For 3D thin shells, the most common formulation is the (\mathbf{T}, Φ) one especially because only the superconducting shell needs to be modeled [10] [11] [12].

Therefore, a quasi three-dimensional model has been implemented in the in-house CAST3M finite element code [13], using the (\mathbf{T}, Φ) formulation.

Section 2 details the mathematical formulation of the problem and the developments performed in CAST3M. These developments include new operators taking into account the superconducting behavior of the material and the anisotropic dependence of the current density on the magnetic induction.

Section 3 covers the modelling of screening currents computed in 3D using simple quasi-infinite straight tape and single loop models. These 3D models were subsequently benchmarked against analytical formulae.

Finally, in section 4, a larger model was analysed using this formulation in order to compute the SCIF of a small solenoid, depending on its winding, made either of layers or pancakes. The results have also been compared to the calculation of the SCIF with a more simple 2D model made of nested turns.

II. PRESENTATION OF THE SCREENING CURRENT MODEL

A. Mathematical formulation of the problem

The first and main equation driving the problem of screening currents is Faraday's equation, stated in (1) in terms of the vector potential \mathbf{A} . \mathbf{E} is the electrical field and V the electrostatic potential.

$$\mathbf{E} = -\dot{\mathbf{A}} - \nabla V \quad (1)$$

\mathbf{A} is the sum of the self vector potential, generated by the \mathbf{J} distribution within the model, and of an external vector potential, from an external source, $\mathbf{A} = \mathbf{A}_{\text{self}} + \mathbf{A}_{\text{ext}}$.

To this equation, we add Ohm's law (2), that links the electrical field \mathbf{E} and the current density \mathbf{J} with the resistivity of the material ρ .

$$\mathbf{E} = \rho \mathbf{J} \quad (2)$$

The HTS tapes we need to study are very thin, around $1 \mu\text{m}$ (thickness of the superconducting layer) and therefore, they can be considered as thin shells. In addition, as the conservation of electric charge on a surface S follows $\nabla_s \cdot \mathbf{J} = 0$, we can write \mathbf{J} in terms of the electric vector potential \mathbf{T} , $\mathbf{J} = \nabla_s \times \mathbf{T} = \nabla_s T \times \mathbf{n}$ (where $\nabla_s \cdot V$ and $\nabla_s \times \mathbf{V}$ are the surfacic divergence and surfacic curl of \mathbf{V} respectively). T is the modulus of \mathbf{T} and \mathbf{n} is the unit vector normal to the surface S .

By using the Biot-Savart formula (3) that links the current density \mathbf{J} within the sample and the self vector potential \mathbf{A}_{self} , the equation for \mathbf{T} is shown in (4).

$$\mathbf{A}_{\text{self}}(\mathbf{r}) = \frac{\mu_0}{4\pi} \int_S \frac{\mathbf{J}(\mathbf{r}')}{|\mathbf{r} - \mathbf{r}'|} dS' \quad (3)$$

$$\rho \nabla_s \times \mathbf{T} + \frac{\mu_0}{4\pi} \frac{\partial}{\partial t} \int_S \frac{\nabla_s \times \mathbf{T}(\mathbf{r}')}{|\mathbf{r} - \mathbf{r}'|} dS' = -\frac{\partial \mathbf{A}_{\text{ext}}}{\partial t} - \nabla_s V \quad (4)$$

B. Superconducting behavior

Equation (4) holds for a conductor with a resistivity ρ and is commonly used to compute eddy currents in thin shells.

To take into account the particular behavior of the superconducting material, we use the well-known power law shown in (5), linking the electrical field E to the current density \mathbf{J} . J_c is the critical current density and n is the n-factor usually set between 25 and 30 for HTS conductors. E_0 is a constant usually defined at $10^{-4} V m^{-1}$.

$$E = E_0 \left(\frac{|\mathbf{J}|}{J_c} \right)^n \quad (5)$$

Hence, the equivalent resistivity of the HTS conductor is derived from (5):

$$\rho = E_0 \left(\frac{|\mathbf{J}|}{J_c} \right)^{n-1} \frac{1}{J_c} \quad (6)$$

HTS conductors show an anisotropic dependence of J_c on B , both on magnitude and orientation. It has been shown that an elliptical functional form of J_c presented in (7) is capable of reproducing accurately [14] experimental characterizations of tapes. B_{\parallel} and B_{\perp} are the parallel and orthogonal components of the field to the tape respectively. J_{c0} , k , b and B_c are four parameters needed to fit experimental data.

$$J_c(B_{\parallel}, B_{\perp}) = \frac{J_{c0}}{(1 + \sqrt{(kB_{\parallel})^2 + B_{\perp}^2}/B_c)^b} \quad (7)$$

C. Resolution with CAST3M

The first step to calculate screening currents in superconductors is to choose an adequate state variable and to solve it. Once this state variable is solved for the initial state and temporal conditions, the current density and SCIF can be calculated.

Thus, to solve (4), we use a finite element method within the CAST3M code [15]. The method with a constant resistivity ρ (eddy currents problem in thin shells) is already implemented in CAST3M and has been described in detail in [16]. It takes into account a weak formulation of the problem (Galerkin method) and the nodal equation associated is:

$$[R]T + [M] \frac{\partial T}{\partial t} = -\frac{\partial \psi_{\text{ext}}}{\partial t} \quad (8)$$

T is the vector of nodal current function values and is the state variable to be solved. R is the resistance matrix, that depends on the resistivity ρ .

M is the mutual-inductance matrix linked to the A_{self} contribution.

The current density vector potential T is an orthogonal curl-conform 1-form, associating values of the potential to vectors normal to the superconducting tape S . For practical purposes in CAST3M, this will be represented by a nodal vector field \mathbf{T} . The latter represents a 0-form defined on the tape which values correspond to the values of the 1-form associated with the local unit normal to the tape $\mathbf{T}(\mathbf{r}') = T(\mathbf{r}') \mathbf{n}_{\mathbf{r}'}$. We opt to discretize the \mathbf{T} field using basis functions linear in the mesh elements. This results in $\mathbf{J} = \nabla_s \times \mathbf{T}$ being constant within each elements. Therefore, considering a mesh partition of the tape which we call S and from established in 4:

$$\begin{aligned} \frac{\partial \mathbf{A}_{\text{self}}}{\partial t} &= \frac{\mu_0}{4\pi} \int_S \frac{1}{|\mathbf{r} - \mathbf{r}'|} \frac{\partial (\nabla_s \times \mathbf{T}(\mathbf{r}'))}{\partial t} dS' \\ &= \frac{\mu_0}{4\pi} \sum_{s_e \in S} \left(\int_{s_e} \frac{ds_e}{|\mathbf{r} - \mathbf{r}'|} \nabla_{s_e} \times \frac{\partial \mathbf{T}(\mathbf{r}')}{\partial t} \right) \\ &= \frac{\mu_0}{4\pi} \sum_{s_e \in S} \left(\int_{s_e} \frac{\nabla_{s_e} \times \mathbf{n}_{s_e} ds_e}{|\mathbf{r} - \mathbf{r}'|} \right) \end{aligned}$$

We have $\mathbf{T}(\mathbf{r}') = T(\mathbf{r}') \mathbf{n}_{\mathbf{r}'}$, thus $\nabla \times \mathbf{T}(\mathbf{r}') = T(\mathbf{r}') \nabla \times \mathbf{n}_{\mathbf{r}'} + \nabla T(\mathbf{r}') \times \mathbf{n}_{\mathbf{r}'}$. In a triangular element s_e , because the normal to the element and the gradient of T are constant, $\nabla \times \mathbf{T}(\mathbf{r}') = \nabla T(\mathbf{r}') \times \mathbf{n}_{s_e}$. Therefore:

$$\begin{aligned} \frac{\partial \mathbf{A}_{\text{self}}}{\partial t} &= \frac{\mu_0}{4\pi} \sum_{s_e \in S} \int_{s_e} \left(\frac{ds_e}{|\mathbf{r} - \mathbf{r}'|} \right) \mathbf{n}_{s_e} \times \nabla \left(\frac{\partial T}{\partial t} \right) \\ &= M \cdot \frac{\partial T}{\partial t} \end{aligned}$$

The most important thing in the computation of the matrix of mutual inductions M is to proceed carefully with the integration of the Green kernel. In the case of the source point \mathbf{r}' being in the same element as the target point \mathbf{r} , the integration is evaluated analytically. Otherwise, a simple numerical quadrature is enough since there is no risk of singularity. Additionally, as long as the geometry and the mesh do not change during the simulation, the dense matrix M stays also constant.

R is also dependent on the model used and is calculated once as it remains constant for a usual eddy current problem. $\frac{\partial \psi_{\text{ext}}}{\partial t}$ is the known vector containing the variations of the external magnetic field that induce the eddy currents.

To solve our problem, we had to develop procedures to take into account the superconducting behavior of the tape, *i.e.* power law and dependence of J_c on the magnetic field. We developed a procedure to compute the field at each node from a known distribution of the current function T ; other procedures were made to calculate the critical current density J_c from the magnetic field distribution and to compute the distribution of the resistivity ρ and consequently the R matrix.

To resolve the partial differential equation (8) in the time domain, we used the Crank-Nicolson method as it is unconditionally stable. The system of equations to solve (8) therefore becomes:

$$\begin{aligned} & \left([M] + \frac{\Delta t}{2} [R^{n+1}] \right) T^{n+1} = \\ & \left([M] - \frac{\Delta t}{2} [R^n] \right) T^n - \frac{\Delta t}{2} \left(\frac{\partial \psi_{ext}^{n+1}}{\partial t} + \frac{\partial \psi_{ext}^n}{\partial t} \right) \end{aligned} \quad (9)$$

Where the unknown is T^{n+1} , which is the vector holding the nodal values of the current function at the (n+1)-th time step. Thus, the determination of the final solution at each time step requires the computation of several iterates of T_k^{n+1} using the sequential Picard's method [17]:

$$\begin{aligned} & [M] T_{k+1}^{n+1} = [M] T^n - \\ & \frac{\Delta t}{2} ([R^n] T^n + [R_k^{n+1}] T_k^{n+1}) - \frac{\Delta t}{2} \left(\frac{\partial \psi_{ext}^{n+1}}{\partial t} + \frac{\partial \psi_{ext}^n}{\partial t} \right) \end{aligned} \quad (10)$$

The sequence of T_k^{n+1} is initialized for the first iteration with T^n ($T_0^{n+1} = T^n$). It converges after a few iterations and the process is eventually stopped whenever the difference between two consecutive estimates drops below a prescribed tolerance $|T_{k+1}^{n+1} - T_k^{n+1}| < \epsilon$. The value of T_{k+1}^{n+1} is then kept as the final solution T^{n+1} .

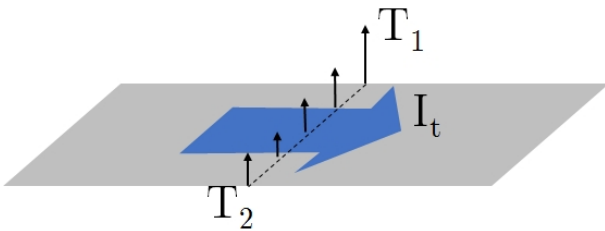


Fig. 1. Representation of the transport current and the electric vector potential in a thin tape. The electric vector potential is normal to the surface and constant on the boundaries of the model.

As there is no current flowing out of the edges of the surface S , the current function T is constant on the boundaries of S . Moreover, if we integrate the current density \mathbf{J} over the section of a tape as shown in Fig. (1), we demonstrate that the current flowing into it is the difference of the two values of the potential vector T at its boundaries:

$$\mathbf{I} = \int_S \mathbf{J} \cdot d\mathbf{S} = \int_S (\nabla_s \times \mathbf{T}) \cdot d\mathbf{S} = \oint_l \mathbf{T} \cdot d\mathbf{l} = T_1 - T_2 \quad (11)$$

To charge a tape with a defined current evolution, we just set a null value on one boundary and the defined current evolution with time on the other.

III. BENCHMARKS OF SIMPLE CONFIGURATIONS

In order to assess the validity of codes, it is of great interest to develop benchmarks. In this section, we present two simple scenarios, the calculation of the distribution of the current density within an infinite thin straight tape and within a single thin loop. The first one is based on analytical formulations and could be re-used by others researchers.

Using the new developed procedures in CAST3M, we computed the screening currents and benchmarked them successfully against these two scenarios.

A. Infinite thin tape with constant critical current density

The generation of screening currents within an infinite tape provides a convenient starting point for benchmarking, as it can be formulated analytically assuming a constant critical density J_c and a critical-state model (CSM) law [18]. Zeldov developed these analytical formulae [19] for a thin film initially in a virgin state subjected to a successive increase and decrease of the transport current.

The distribution of the sheet current density $J(x)$ obtained over the width of the tape when the total supplied current is increased from 0 to I_t is represented in the following two equations:

$$J(x) = \begin{cases} \frac{2J_c}{\pi} \arctan \left(\sqrt{\frac{w^2 - a^2}{a^2 - x^2}} \right) & \text{for } -a < x < a \\ J_c & \text{for } a \leq |x| < w \end{cases} \quad (12)$$

with $a = w\sqrt{1 - (I_t/I_c)^2}$ and $I_c = 2dwJ_c$. w and d are the half-width and the thickness of the tape respectively. J_c is the critical current density, assumed to be constant and uniform, and I_c the related critical current of the tape.

The current density distribution obtained over the tape width $J(x)$ after a decrease of the supplied current from I_t to $I_{t0} = I_t - \Delta I_t$ is represented by the following three equations:

$$J(x) = \begin{cases} \frac{2J_c}{\pi} \left[\arctan \left(\sqrt{\frac{w^2 - a_0^2}{a_0^2 - x^2}} \right) - 2 \arctan \left(\sqrt{\frac{w^2 - a^2}{a^2 - x^2}} \right) \right] & \text{for } -a_0 \leq x \leq a_0 \\ J_c \left[1 - \frac{a}{\pi} \arctan \left[\left(\sqrt{\frac{w^2 - a^2}{a^2 - x^2}} \right) \right] \right] & \text{for } a_0 \leq |x| \leq a \\ -J_c & \text{for } a \leq |x| < w \end{cases} \quad (13)$$

with $a_0 = w(1 - I_{t0}/I_c)$ and $a = w(1 - \Delta I_t/2I_c)$ for $\Delta I_t \leq 2I_{t0}$.

These formulae have been set up for the critical-state law which is different from the power law used in CAST3M. The critical-state model cannot describe relaxation effects or over-current effects; the calculation performed with the critical-state law is especially insensitive to the ramping rate magnitude of the current and depends only on the final value I_t . This is not the case for computations performed with the power law as the electrical field depends on the current density. Nevertheless, the computations are valid only for a current density from 0

TABLE I
PARAMETERS FOR THE INFINITE TAPE MODEL

Parameter		Unit	Value
Number of elements	n_e		4364
Tape half-width	w	mm	6
Tape thickness	d	μm	1
Critical current density	J_c	A mm^{-2}	10^{10}
Critical current	I_c	A	120
Ramp-up time	t_u	s	1
Ramp-down time	$t_d - t_u$	s	1
Current @ t_u	I_t		70% I_c

to J_c and just above it (flux-creep regime) as the flux-flow regime, occurring at $J > J_c$, is not properly described with the power law.

We then computed three cases with the exact same hypotheses except for the n-value that we progressively increased from 25 (realistic case for HTS) to 500 (close to the CSM). A power law with a very high n-value does not have a real physical meaning for HTS conductors but allows to approach the CSM law. Fig. (2) shows $E(J)$ characteristics for the CSM and the power law.

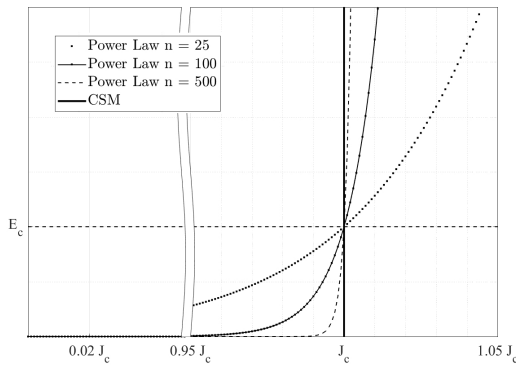


Fig. 2. $E(J)$ characteristics. The CSM is represented by the thick line at J_c . The power law is represented for three values of the n-factor, 25, 100 and 500 used in the 2D computations, for comparison with the CSM.

We also performed the same calculations with a 2D in-house code developed in MATLAB and based on a (A, V) formulation described in (1)[7]. The computations have been led for a thin tape with only one element in the thickness to be representative of the formulation.

This simple scenario based on analytical formulations is a useful benchmark to test codes and assess their validity. The code should be able to handle computations with a very high n-factor to mimic the CSM.

The parameters used for the computations are listed in table (I). The CAST3M model, represented in Fig. (3), is a tape with a finite length, defined as more than 10 times the value of its width to exclude boundary effects. The mesh is densified at the center of the model, in order to detail the sheet current density distribution across the tape. The transport current evolution with time is shown in Fig. (4). The distribution of the current density is shown at time t_u in Fig. (5). There is a very good agreement between the CAST3M and the MATLAB results. When increasing the n-value, the



Fig. 3. CAST3M model used for the infinite straight tape computations.

two distributions, obtained either with CAST3M or MATLAB, tend to the critical-state results. A very good agreement is reached at an n-value of 500. It is to be noted that the lower the n-value, the more the results are sensitive to the current slope. This is interesting because, as the n-value is low in HTS materials, increasing the transport current with a smaller slope will generate a more uniform current density distribution as shown in Fig. (4) and consequently a reduced SCIF.

The distribution of the current density is shown at time t_d after a ramp-up ramp-down cycle in Fig. (6). There is still a very good agreement between CAST3M and MATLAB at every n-value; for a n-value of 500, the computations, either performed with CAST3M or MATLAB, show very good agreement with the analytical formulae (13). Computations of screening currents in publications show also similar distribution of the current density, for instance Fig. 9.a of [20].

Finally, several factors may influence the current density distribution and consequently the SCIF. First, the thickness of the superconducting layer has no influence because the geometry is modelled as a thin shell. Second, as shown in (12) and (13), the current density distribution depends on the ratio a/w which is constant for a given operation current I_t . Increasing the width $2w$ will enlarge by homothety the current density distribution and consequently if we compare the magnetic field generated from this distribution to the magnetic field due to an uniform distribution, the ratio will remain the same. Obviously, the SCIF is reduced if we subdivide the tape in several smaller tapes, well-known technique to lower the magnitude of AC losses related to SCIF.

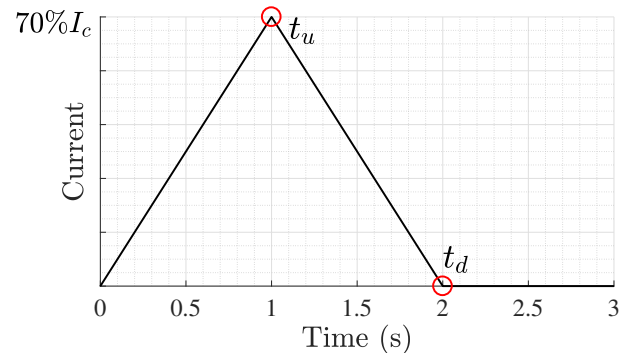


Fig. 4. Evolution of the transport current with time. The transport current is increased from 0 A (tape in a virgin state) to 70% of the critical current of the tape (time t_u). Then, the current is decreased back to zero (time t_d).

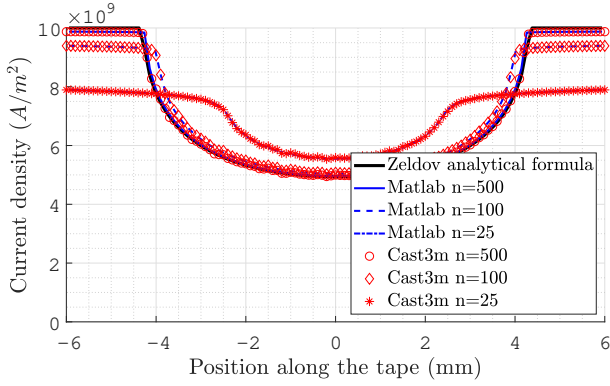


Fig. 5. Distribution of the current density across the width of a tape. The transport current is increased from zero to a final value I_t in a sample initially in a virgin state (time t_u of Fig. (4)). The black line represent the analytical formula developed by Zeldov. The blue lines are the results of the 2D computations performed with MATLAB. The red symbols are the results of the 3D computations performed with CAST3M.

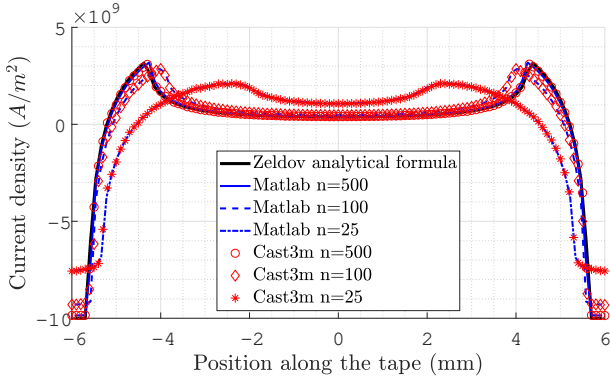


Fig. 6. Distribution of the current density across the width of a tape. The transport current is increased from a sample initially in a virgin state to a value I_{t0} and then decreased to $I_t = 0$ (time t_d of Fig. (4)). The black line represents the result obtained through the analytical formula developed by Zeldov. The blue lines are the results of the 2D computations performed with MATLAB. The red symbols are the results of the 3D computations performed with CAST3M.

B. Single loop with variable critical current density

To validate completely the new procedures, we need to benchmark them with a J_c dependence on the magnetic induction. The second simple case is therefore a single loop with a critical current density J_c dependent on the magnetic induction according to the elliptic law described in (7). The corresponding meshed geometry used in CAST3M is shown in Fig. (7).

We compare the CAST3M and MATLAB results obtained for the same transport current evolution as in the former problem (see Fig. (4)). The MATLAB model is made of only one element in its thickness.

Numerical values used for the model parameters are listed in table (II).

Results are shown in Fig. (8) and Fig. (9); they show complete agreement between CAST3M and MATLAB. The current density distribution is different from the former case especially at the edges of the tape. This is the consequence of the use of the elliptic law for J_c : as the orthogonal field is

TABLE II
PARAMETERS FOR THE LOOP MODEL

Number of elements	n_e		1848
Tape half-width	w	mm	6
Tape thickness	d	μm	1
Ramp-up time	t_u	s	1
Ramp-down time	t_d	s	1
Current @ t_u	I_t		70% I_c
Elliptic fit	(cf. (7))		
	J_{c0}	A mm^{-2}	10^{10}
	k		0.25
	B_c	mT	25
	b		0.6

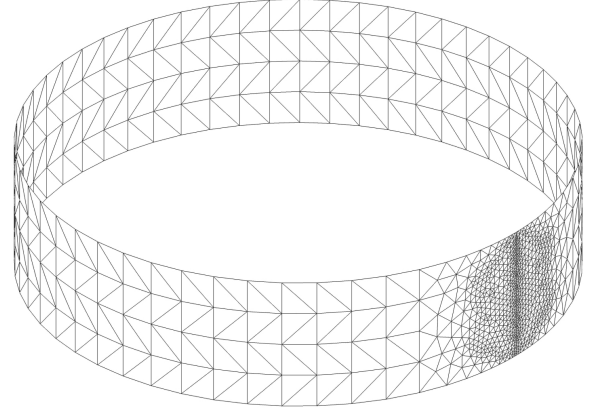


Fig. 7. CAST3M Model used for the single loop computations.

the strongest at the edges of the tapes, the local value of the critical current density J_c is consequently reduced there.

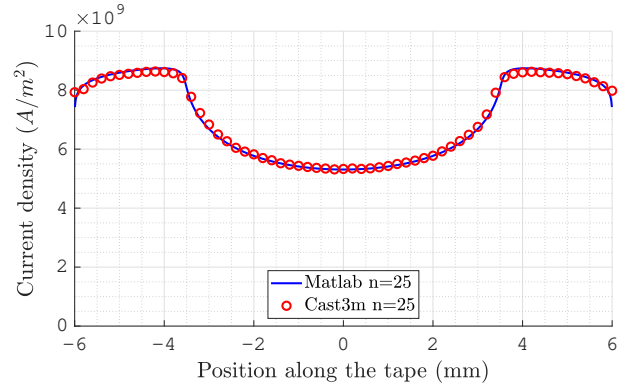


Fig. 8. Distribution of the current density across the width of a turn. The transport current is increased from zero in a sample initially in a virgin state to a value I_t (time t_u of Fig. (4)). The blue line is the result of the 2D computations performed with MATLAB. The red symbols are the results of the 3D computations performed with CAST3M.

We conducted a study to find out how the computation time scales with the number of nodes in CAST3M for this 3D case. The computations were done with a computer with Intel(R) Xeon(TM) CPU E5-2637 bi-processor at 3.50 GHz with 128 GB RAM. Fig. (10) shows the computation time measured for the calculation of the inductance matrix M and for the calculation of the current density. The study shows a power law dependence (exponent close to 2) of the computation time in seconds with the number of nodes as it is quasi-linear in

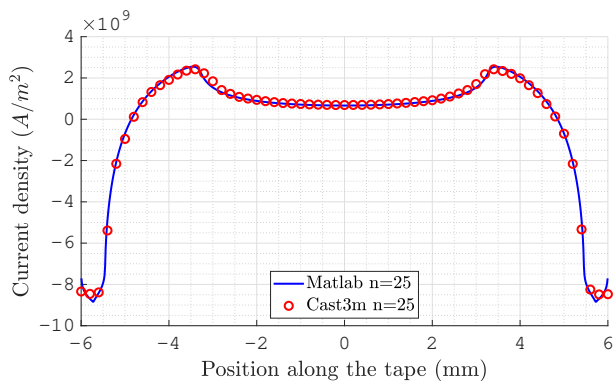


Fig. 9. Distribution of the current density across the width of a turn. The transport current is increased from zero in a sample initially in a virgin state to a value I_{t0} and then decreased to $I_t = 0$. (time t_d of Fig. (4)). The blue line is the result of the 2D computations performed with MATLAB. The red symbols are the results of the 3D computations performed with CAST3M.

the log-log plot of the current density computation. It takes more than 30 hours to compute a problem with a model of 11000 nodes. This is consistent with the resolution time needed for similar problems [20]. We also measured the time needed for the same problem solved with MATLAB in 2D. The time needed for the inductance matrix computation or the current density computation are lower than 1 and 10 seconds, respectively.

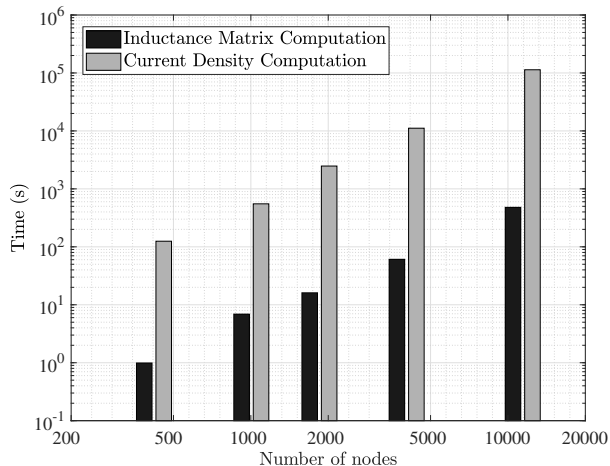


Fig. 10. Computation time in seconds as a function of the number of nodes for the single loop model. The plot is in log-log scale and is quasi linear. There is indeed a power law dependence with a power exponent close to 2 for the current density computation plot.

These two simple cases show that the new procedures implemented in CAST3M are valid and that we can use it on larger models with confidence.

IV. COMPARISON OF SCIF GENERATION BETWEEN LAYER-WOUND AND PANCAKE COILS

In this section, we compare the influence of the winding type used for a solenoid on the generation of screening currents and SCIF. This is a typical 3D problem which is of great interest, especially for domains (NMR, MRI) where homogeneity and stability of the magnetic field are required.

TABLE III
DATA FOR THE 3D MODELS

Type of winding		Pancakes	Layers
Number of elements	n_e	10500	10500
Tape width (mm)	w	12	12
SC tape thickness (μm)	d	1	1
Total length of SC tape (m)	l_t	3.96	3.93
Internal diameter (mm)	ϕ_i	48	48
Space between pancakes/turns (mm)	h	1	1
Magnetic field constant ($\mu\text{T A}^{-1}$)	α	379.1	380.6

TABLE IV
DATA FOR SC MATERIAL

Power law	n-value	n		25
Elliptic fit	(cf. (7))			
		J_{c0}	A mm^{-2}	10^{10}
		k		0.25
		B_c	mT	25
		b		0.6

To have a point of reference, we compare the results with a 2D problem performed with MATLAB; the winding in that case is equivalent to a set of nested turns due to the axisymmetry. The method of computation for the 2D case is similar to the one used in [7].

The two models used in CAST3M are shown in Fig. (11). Both are made of 5 layers/pancakes of 5 turns. The total number of elements for each model is 10500 which is already a large model as the $[M]$ matrix defined in (8) is a dense square matrix with 10500×10500 elements.

The main parameters used for the model are listed in table (III). Although their design is different, the total length needed for the winding is almost the same. The comparison is however difficult as we do not take into account the junctions between layers/pancakes. The magnetic field constant values, 379.1 and 380.6 $\mu\text{T A}^{-1}$ for the pancake model and the layer model respectively, are very similar with less than 0.5% of difference. For comparison, the magnetic constant of the 2D model made of nested turns is 383.3 $\mu\text{T A}^{-1}$.

The data used for the superconducting material and the elliptic law are listed in table IV.

It takes more than 32 hours to calculate completely the evolution of current function distribution within the models. This very substantial computational time is the main drawback of the method used. For several geometrical configurations, it is possible to avoid meshing the whole tape domain by exploiting the helical symmetry of the model [21]. In that case, the state variable to solve is the current density J and the first order equation is similar to our 2D computations [7]. For comparison, it takes 85 s with MATLAB to compute the whole problem with the nested turn model.

Fig. (12) shows the evolution with current of the SCIF at the center of the coils. For the three models, we see an increase of the SCIF up to a maximum, when the current is ramped up, followed by a decrease. The maximal magnitude of the SCIF is 1 and 1.37 mT for the layer model and the pancake model respectively, representing 8.3% and 4.7% of the total magnetic field.

During the first part, the transport current I_t is much

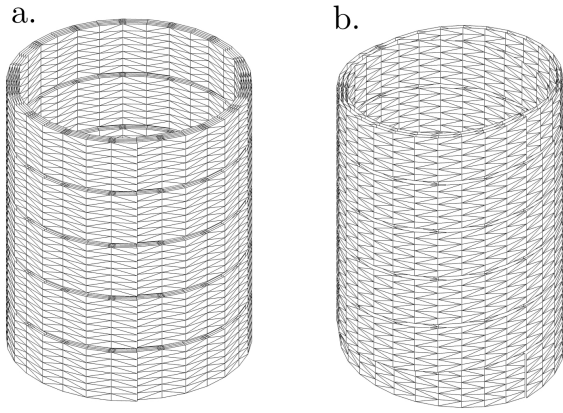


Fig. 11. Coil models used for the computations. a. is a coil made of 5 pancakes of 5 turns. b. is a coil made of 5 layers of 5 turns. Each model has 10500 elements.

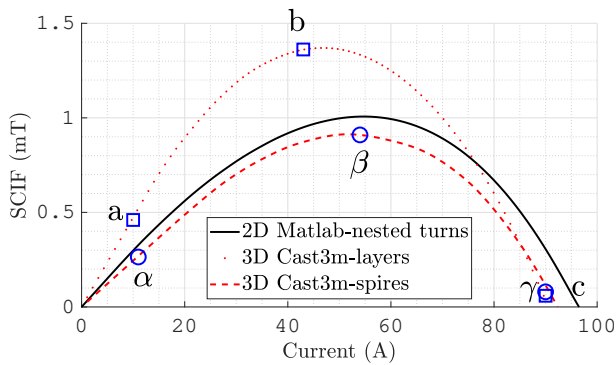


Fig. 12. Evolution of the SCIF at the center of the coils with the current. The red dotted line represents the computations performed with CAST3M for the layer wound coil model. The red dashed line represents the computations performed with CAST3M for the pancake wound coil model. The solid black line is the result for the computations in 2D (nested coils) with MATLAB. The distribution of the current density is shown in Fig. (13) and Fig. (14) at points (a, b, c) and (α , β , γ).

lower than the critical current I_c and the influence of the screening currents on the generation of the magnetic field is the strongest. This can be seen in Fig. (13) and Fig. (14) where the distribution of the current density within the tapes are not uniform at all, especially at the maximum value of the SCIF (b and β).

Then, as the transport current continues to increase, two phenomena start occurring simultaneously. First, the increase of the transport current generates a larger magnetic field and consequently the critical current density decreases due to its dependence on the magnetic field (cf. (7)). Second, the ratio of the transport current to the critical current is larger and the tape tends to a complete uniform current density distribution, as shown in Fig. (13) and Fig. (14). The SCIF consequently decreases under these two influences and vanishes when the tape current is close to its critical value (c and γ).

Moreover, we observe that the current density distributions are both symmetrical with respect to the median plane but are very different. There is a strong distortion of the magnetic flux in the layer-wound model. The gaps between conductors in a given layer twist the self-generated magnetic flux with the

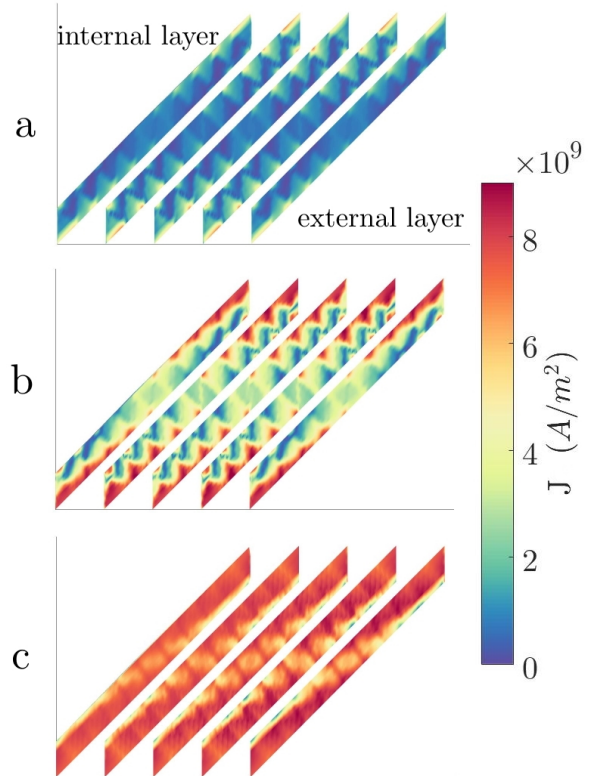


Fig. 13. Distribution of the current density for a layer-wound coil for different transport current values (see Fig. (12)). The layers have been unwound for visualization. The internal one is the left and the external one on the right.

consequence of a periodic distribution of the current density J which depends on the local critical current density J_c and consequently on the magnetic field as described in (7). This periodicity is 10 as shown in Fig. (14), corresponding to the number of cross zones between two layers of 5 turns. This phenomenon is similar to the results of the current density distribution for spiraled conductors [22].

The distribution of the current density of the pancake model does not exhibit these patterns. The magnetic flux is not distorted and its distribution tends to the 2D model one, already seen in similar computations of the current density distribution [23].

The maximum SCIF value is larger for the layer-wound coil by more than 50%, although their magnetic constants are similar, and occurs at a smaller value of the transport current. This is a little bit surprising as we were expecting that the layers would shield more than the pancakes against the variation of the magnetic field. The layer shape is indeed similar to a magnetic shield, whose efficiency has been reported in [24]. Nevertheless, our model is different as the current density distribution is not only driven by an external source (electromotive force) like in the case of an independent shield. The generation of SCIF with models made of a larger number of turns should be compared in order to confirm this tendency.

Moreover, the MATLAB and CAST3M computations are very similar in the case of the pancake structure with just a small overestimation of the SCIF with the 2D code and

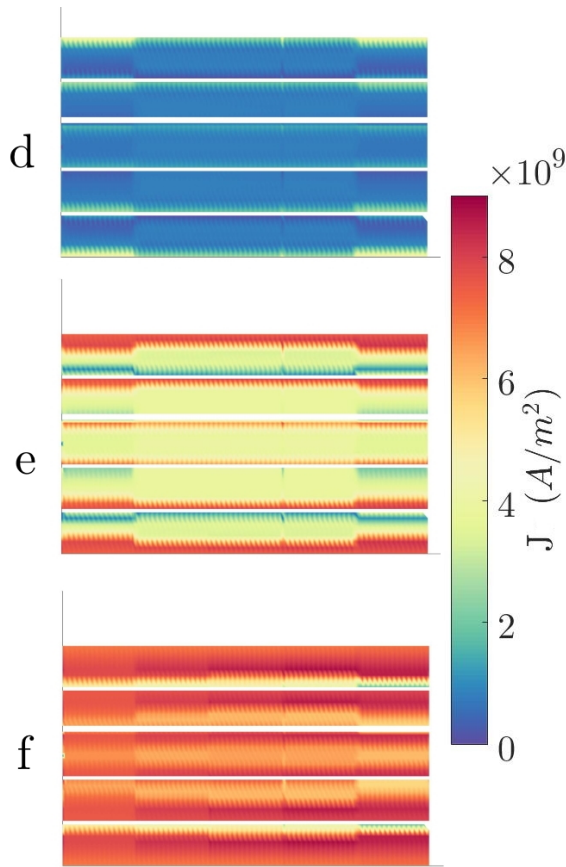


Fig. 14. Distribution of the current density for a coil made of pancakes for different transport current values (see Fig. (12)) The pancakes have been unwound for visualization. The internal radius of each pancake is on the left and the external radius on the right.

the nested coils. This is the consequence of the similarity of the distributions of their magnetic field, as stated *supra*. We then could use the 2D code when calculating SCIF with pancakes coils, saving a substantial computation time, from days to seconds.

V. CONCLUSION

We have developed a useful tool for calculating screening currents in REBCO tapes for 3D shape configurations especially the ones that cannot be reducible to 2D models. It is based on existing procedures of the in-house code CAST3M to which we added new procedures that take into account the characteristics of superconductors.

Simple scenarios have been defined to benchmark the code and assess the validity of the new procedures. The simpler one is based on the CSM model with a constant critical current density and led to analytical formulations; it could be used by others researchers to test their own code. CAST3M has been benchmarked successfully against these formulations.

Then, we studied a case of great interest, especially for domains where homogeneity and temporal stability are required. We computed the screening current distribution in small 3D coils and calculated the SCIF at their center. Two kinds of winding, layers and pancakes, have been investigated that can

only be processed accurately by 3D computations. The results show a large difference as the SCIF generated within the layer wound coil is 50% larger than the SCIF generated by the pancake wound coil. This tendency should be confirmed on windings with a larger number of turns.

The drawback of the 3D calculations is that their computation time is very large compared to simpler 2D models. For the pancake case, we compared CAST3M results for the SCIF with the MATLAB results for a set of nested turns (2D model of the simplified 3D pancake model). There is a slight overestimation of the SCIF with the 2D model, which is related to the difference of the geometry as the magnetic constant for the 2D model is also larger than the one of the 3D model. Nevertheless it should be used as our design tool due to the large computation time saved. For particular geometrical configurations, especially in case of symmetry or periodicity (helix), the problem is also reducible to 2D computations.

REFERENCES

- [1] L. Rossi, A. Badel, Hugues, Bajas et al. The EuCARD2 Future Magnets Program for Particle Accelerator High-Field Dipoles: Review of Results and Next Steps. *IEEE Transactions on Applied Superconductivity*, 28:1–10, 2018.
- [2] Satoshi Awaji, Kazuo Watanabe, Hidetoshi Oguro, Hiroshi Miyazaki, Satoshi Hanai, Taizo Tosaka and Shigeru Ioka. First performance test of a 25 T cryogen-free superconducting magnet. *Superconductor Science and Technology*, 30:065001, 2018.
- [3] Taizo Tosaka, Hiroshi Miyazaki, Sadanori Iwai, Yasumi Otani, Masahiko Takahashi, Kenji Tasaki, Shunji Nomura, Tsutomu Kurusu, Hiroshi Ueda, So Noguchi, Atsushi Ishiyama, Shinichi Urayama and Hidenao Fukuyama. Project Overview of HTS Magnet for Ultra-high-field MRI System. *Physics Procedia*, 65:217–220: 2015.
- [4] F. Grilli, R. Brambilla, and L. Martini. Modeling high-temperature superconducting tapes by means of edge finite elements. *IEEE Transactions on Applied Superconductivity*, vol. 17, no. 2, pp. 3155–3158, Jun. 2007
- [5] T. W. Preston and A. B. J. Reece. Solution of 3-dimensional eddy current problems: The T method. *IEEE Transactions on Magnetics*, vol. MAG18, no. 2, pp. 486–491, Mar. 1982.
- [6] A. Stenvall and T. Tarhasaari. An eddy current vector potential formulation for estimating hysteresis losses of superconductors with FEM. *Superconductor Science and Technology*, vol. 23, no. 12, p. 125013, Dec. 2010.
- [7] Philippe Fazilleau, Franck Borgnolutti, Guillaume Dilasser and Maria Durante. Screening Currents Within the EuCARD HTS Dipole. *IEEE Transactions on Applied Superconductivity*, 28:1–5, 2018.
- [8] Guillaume Dilasser, Philippe Fazilleau, and Pascal Tixador. Experimental Measurement and Numerical Simulation of the Screening Current-Induced Field Decay in a Small REBCO Coil. *IEEE Transactions on Applied Superconductivity*, 27(4), JUN 2017.
- [9] Guillaume Dilasser, Philippe Fazilleau and Pascal Tixador. Investigation on Two Techniques for the Reduction of Screening Current-Induced Field Effects in REBCO HTS Coils. *IEEE Transactions on Applied Superconductivity*, 28(4)1–5, June 2018.
- [10] K. Takeuchi, N. Amemiya, T. Nakamura, O. Maruyama and T. Ohkuma. Model for electromagnetic field analysis of superconducting power transmission cable comprising spiraled coated conductors. *Superconductor Science and Technology*, vol. 24, no. 8, p. 085014, Jul. 2011.
- [11] S. Noguchi, S. Hahn, H. Ueda, S. Kim and A. Ishiyama. An Extended Thin Approximation Method to Simulate Screening Current Induced in REBCO Coils. *IEEE Transactions on Magnetics*, vol. 54, no. 3, pp. 1–4, March 2018.
- [12] Y. Li et al. Influence of E–J Characteristics of Coated Conductors and Field Ramp-Up Rates on Shielding-Current-Induced Fields of Magnet. *IEEE Transactions on Applied Superconductivity*, vol. 28, no. 3, pp. 1–5, April 2018.
- [13] <http://www-cast3m.cea.fr/>.
- [14] F. Grilli, F. Sirois, V. M. R. Zermeno and M. Vojenciak. Self-Consistent Modeling of the I_c of HTS Devices: How Accurate do Models Really Need to Be? *IEEE Transactions on Applied Superconductivity*, 24(6):1–8, 2014.

- [15] Pierre Verpaux, Thierry Charras, and Alain Millard. Castem 2000 une approche moderne du calcul des structures. *Calcul des structures et intelligence artificielle*, page 261–271, 1988.
- [16] J. Blum, L. Dupas, C. Leloup and B. Thooris. Eddy Current Calculations for the Tore Supra Tokamak. *IEEE Transactions on Applied Superconductivity*, 19(6):2461–2464, 1983.
- [17] Emile Picard, Académie des Sciences. Comptes rendus hebdomadaires des séances de l'Académie des sciences. *Gauthier-Villars (Paris)*, (118) 454–458, 1894.
- [18] P.W. Anderson and Y.B. Kim. Hard Superconductivity - Theory of Motion of Abrikosov Flux Lines. *Reviews of Modern Physics*, 36(1P1):39–&, 1964.
- [19] E. Zeldov, J.R. Clem, M. McElfresh and M. Darwin. Magnetization and transport currents in thin superconducting films. *Phys. Rev B*, 49(14):9802–9822, 1994.
- [20] M. Nii, N. Amemiya and T. Nakamura. Three-dimensional model for numerical electromagnetic field analyses of coated superconductors and its application to Roebel cables. *Superconductor Science and Technology*, vol. 25, no. 9, p. 095011, Jul. 2012.
- [21] M. Siahraang, F. Sirois, D. N. Nguyen, S. Babic and S. P. Ashworth. Fast Numerical Computation of Current Distribution and AC Losses in Helically Wound Thin Tape Conductors: Single-Layer Coaxial Arrangement. *IEEE Transactions on Applied Superconductivity*, 20(6):2381–2389, Dec. 2010.
- [22] K. Takeuchi et al. Model for electromagnetic field analysis of superconducting power transmission cable comprising spiraled coated conductors. *Superconductor Science and Technology*, vol. 24, no. 8, p. 085014, Jul. 2011.
- [23] R. Itoh, Y. Oga, S. Noguchi, Ha. Igarashi and Hiroshi Ueda. Numerical simulation of screening current distribution in HTS tape of high field magnet. *Physica C: Superconductivity*, 484:300–304: 2013.
- [24] G. Gabrielse and J. Tan. Self-shielding superconducting solenoid systems. *Journal of Applied Physics*, vol. 63, no. 10, pp. 5143-5148, 1988.